A hydrological modelling-based approach for vulnerable area identification under changing climate scenarios

Sonam S. Dash, Dipaka R. Sena, Uday Mandal, Anil Kumar, Gopal Kumar, Prasant K. Mishra and Monika Rawat

ABSTRACT

The hydrologic behaviour of the Brahmani River basin (BRB) (39,633.90 km^2), India was assessed for the base period (1970–1999) and future climate scenarios (2050) using the Soil and Water Assessment Tool (SWAT). Monthly streamflow data of 2000–2009 and 2010–2012 was used for calibration and validation, respectively, and performed satisfactorily with Nash-Sutcliffe Efficiency (E_{NS}) of 0.52–0.55. The projected future climatic outcomes of the HadGEM2-ES model indicated that minimum temperature, maximum temperature, and precipitation may increase by 1.11–3.72 °C, 0.27–2.89 °C, and 16–263 mm, respectively, by 2050. The mean annual streamflow over the basin may increase by 20.86, 11.29, 4.45, and 37.94% under representative concentration pathway (RCP) 2.6, 4.5, 6.0, and 8.5, respectively, whereas the sediment yield is likely to increase by 23.34, 10.53, 2.45, and 27.62% under RCP 2.6, 4.5, 6.0, and 8.5, respectively, signifying RCP 8.5 to be the most adverse scenario for the BRB. Moreover, a ten-fold increase in environmental flow (defined as Q_{90}) by the mid-century period is expected under the RCP 8.5 scenario. The vulnerable area assessment revealed that the increase in moderate and high erosion-prone regions will be more prevalent in the mid-century. The methodology developed herein could be successfully implemented for identification and prioritization of critical zones in worldwide river basins.

Key words | Brahmani River basin, climate change, environmental flow, sediment yield, streamflow, vulnerability

Sonam S. Dash
School of Water Resources,
IIT Kharagpur,
WB, 721302 Kharagpur,
India

Dipaka R. Sena
Uday Mandal (corresponding author)
Gopal Kumar
Prasant K. Mishra
Hydrology and Engineering Division,
ICAR-Indian Institute of Soil and Water Conservation-Dehradun,
Dehradun, Uttarakhand, 248195,
India
E-mail: *uget.uday.mandal@gmail.com*

Anil Kumar
G. B. Pant University of Agriculture & Technology,
Pantnagar, 263145, Uttarakhand,
India

Monika Rawat
Amity University,
Noida, 201301,
India

INTRODUCTION

Water is becoming one of the scarcest natural resources in densely populated countries such as India despite the fact that they are endowed with many seasonal and perennial rivers often causing flood havoc. This warrants close attention of policy makers and implementing agencies responsible for the implementation of sustainable water conservation and management practices. For efficient management of water resources in various sectors such as domestic, irrigation, and industrial sectors, and to improve flood control, drainage, and water quality, an accurate forecast of streamflow is essential. The need for management activities becomes intense in case of severe alteration in the climate and land use pattern of a region. A little variability in the rainfall pattern may cause a substantial impact on agriculture and allied sectors by alteration of the supply-demand scenario in agriculture with changes in streamflow and sediment yield.

The increased weather extremes and uncertainties under climatic change scenarios may render natural resources extremely vulnerable. Though the climate change projections are moderate for the tropical region, the impact of climate change is likely to be adverse, mainly because of the over-dependency on natural resources for ecosystem services, and prevailing relative narrow range of base

doi: 10.2166/wcc.2020.202

temperature (Kumar *et al.* 2017). Streamflow, environmental flow (e-flow), potential soil erosion, and irrigation requirement are susceptible to change under changing climate, and their estimation is crucial for future planning and management of water resources (Adhikary *et al.* 2019). Streamflow in Brahmani River basin (BRB) is reported to be more sensitive to the variation in rainfall than the variation in temperature (Islam *et al.* 2012). Islam reported a significant likely decrease in winter streamflow (i.e. from October to February), which may affect the *Rabi*/winter crop seasons, and subsequently reduce water availability for summer crops. Increased streamflow projected for the monsoon season may lead to extensive flooding conditions. The quantification of soil erosion and identification of critical areas are the prerequisite for the adoption of best management practices to control soil erosion and sustain agricultural production under both present and future climate scenarios. There is an urgent need to quantify the climate change impacts in order to formulate sustainable adaptive measures (Whitehead *et al.* 2009). Temperature extremes are predicted to increase by the end of this century, and a similar trend is expected for precipitation extremes also, particularly over the western part of Central India (IPCC 2001). The projected temperature change under four different representative concentration pathways (RCPs) is likely to vary between 0.5 and 5 °C by the end of this century (IPCC 2013).

For the appraisal of hydrological fluxes, especially under projected climate scenarios, adoption of hydrological models seems to be the only feasible option. The correct choice of model depends on the structure of the model, the purpose of application and availability of model inputs. During the initial phase of hydrological modelling, hydrological processes were reproduced by traditional lumped, conceptual rainfall-runoff models through simplified mathematical equations and for a single layer of storage. A large number of calibration parameters are associated with those models; for example, the Stanford Watershed Model IV (Crawford & Burges 2004) has 16 parameters, and the SACRAMENTO model (Burnash *et al.* 1973) has 21 parameters. These models do not account for various complex phenomena happening inside the basin, and are therefore unable to represent the realistic hydrologic behaviour of the study area.

These drawbacks encouraged the modellers to develop physically based hydrological models such as the SHE model (Abbott *et al.* 1986), Soil and Water Assessment Tool (SWAT; Arnold *et al.* 1998), and the Variable Infiltration Capacity model (VIC; Liang *et al.* 1994). These models are capable enough in representing the physical processes happening inside the catchment with utmost accuracy. However, the poor availability of input datasets at desired spatio-temporal scale remained the primary bottleneck for physically based modelling studies. The SWAT model has emerged as a viable catchment scale modelling tool for quantifying various hydrological fluxes and their influence on corresponding management aspects over a large heterogeneous watershed in a limited data availability scenario (Tripathi *et al.* 2003; Hassan *et al.* 2017; Dash *et al.* 2019). This model is getting continuous support from the United States Department of Agriculture (USDA), Agricultural Research Service (ARS) at the Grassland Soil and Water Research Laboratory, Texas and has become a popular public domain hydrological model. The SWAT model works on the principle of disintegrating the watershed first into sub-watersheds and then into Hydrologic Response Units (HRU) to make it computationally efficient. A better understanding of the calibration parameters describing catchment dynamics may lead to an excellent simulation output with reduced model uncertainty (Lenhart *et al.* 2002).

In the current state-of-the-art, although there are many hydrological modelling-based climate studies in the literature (Hassan 2019; Padhiary *et al.* 2019), no such study is capable of fully mapping the variability in precipitation and temperature of the BRB under changing climate scenarios. Therefore, widespread knowledge about the hydrological fluxes with acceptable certainty can be implemented for possible future impact assessment of BRB. In this study, the output of the HadGEM2-ES climate model is adapted for flow simulation, which is an implementation of CMIP5 centennial simulations.

The BRB is a traditional hub of agricultural activities, but it is converting into an industrial hub as a consequence of rapid urbanization, resulting in significant increase in demand for water. Historically, without prior potential hydrological analysis, the major portion of the available inflow was allocated to less important sectors (Guntner *et al.* 2004). This leads to a significant reduction in the

flow volume at the outlet and intensified water demand at the downstream of the reservoir. Thus, it is necessary to identify the vulnerable areas from the perspective of water demand and severe hydrological alterations. Attempts have been made to quantify the flood hazard (Dash *et al.* 2018) and potential soil erosion-prone regions (Chen *et al.* 2011) individually. The vulnerable areas are a combination of flood and erosion-prone regions because of the complex degree of association between them, which was not addressed in previous studies.

In light of the above research gaps, this study has been carried out with the following specific objectives: (i) to estimate the streamflow and sediment yield fluxes over the BRB under four future climate scenarios; and (ii) to identify the vulnerable sub-basins of the BRB by analysing the streamflow and sediment yield under both present and future climate scenarios. The outcomes of this study will be of great interest to policy makers in selecting the locations for implementing best management practices (BMPs), in order to develop a sustainable operational plan for management of water resources in future climate change scenarios. This paper is organized as follows: In the next two sections information is presented about the study area and the methodology followed in this study is described. The important outcomes of this research are then presented (Results). The paper concludes with important discussions pertaining to the results obtained.

STUDY AREA

The Brahmani River basin is encompassed between longitude 83° 52′ to 87° 30′ E and latitude 20°28′ to 23° 35′ N and constitutes an area of 39,269 km^2 (Figure 1). The basin covers three major Indian states and covers an area of 22,516 km^2 (57%), 15,406 km^2 (39.23%), and 1,347 km^2 (3.77%) in Odisha, Jharkhand, and Chhattisgarh state, respectively. The basin receives input in the form of rainfall as the only natural source and from irrigation as an artificial source. The basin experiences an average annual rainfall of 1,305 mm and about 70% is concentrated during the monsoon period (June–October). The maximum and minimum temperature of 47 °C and 4 °C, respectively, is indicative of the presence of wide ecological variability in the basin. The elevation in the basin ranges between 1 and 1,169 m above mean sea level (MSL) with an area weighted average elevation of 341 m (Figure 1). The basin is characterized by an undulating topography, the average slope being 0.06% in the central part of the basin. Croplands are the major land use class of the basin and comprise 52.04% of the total basin area with permanent water bodies as the lowest land cover class (2.95%). Agriculture is the primary source of livelihood for the people living in this basin and paddy is the major crop cultivated in the basin. The basin is characterized by five major soil groups: loamy soil is the dominant soil group covering 37.2% of the total area followed by clay loam (27.81%), sandy loam (22.17%), sandy clay loam (7.50%), and clay (5.25%) soil (Figure 2(b)).

METHODOLOGY

Hydrological model: SWAT

In SWAT, the inherent spatial heterogeneity involved with the study area is conceptualized through distinct processing units known as sub-basins, and subsequent discretization of these sub-basins results in uneven shaped processing units, Hydrologic Response Units (HRUs). These HRUs are the consequence of the overlay of exclusive land use, soil, and slope classes present in the study area. The effect of various catchment-scale parameters such as available moisture content, hydraulic conductivity, pollutant loading, and management practices on streamflow generation is simulated along the individual HRUs. Further, utilizing appropriate weighted average techniques, the HRU-scale outputs are stacked into sub-basin-scale outputs. The sub-basin-scale hydrological entities are further routed along the complete river reach using two inbuilt routing approaches, variable storage and Muskingum routing techniques. Channel routing is accomplished by the variable storage and Muskingum routing approaches, which are the consequences of the kinematic-wave model (Chow *et al.* 1988). The Muskingum and variable storage routing approach was adopted in SWAT to carry out the channel routing. Vertical soil water characterization is accomplished by four zonal distributions: snow deposition (surface soil), soil water storage, shallow aquifer storage, and deep aquifer storage. Surface runoff estimation in SWAT is

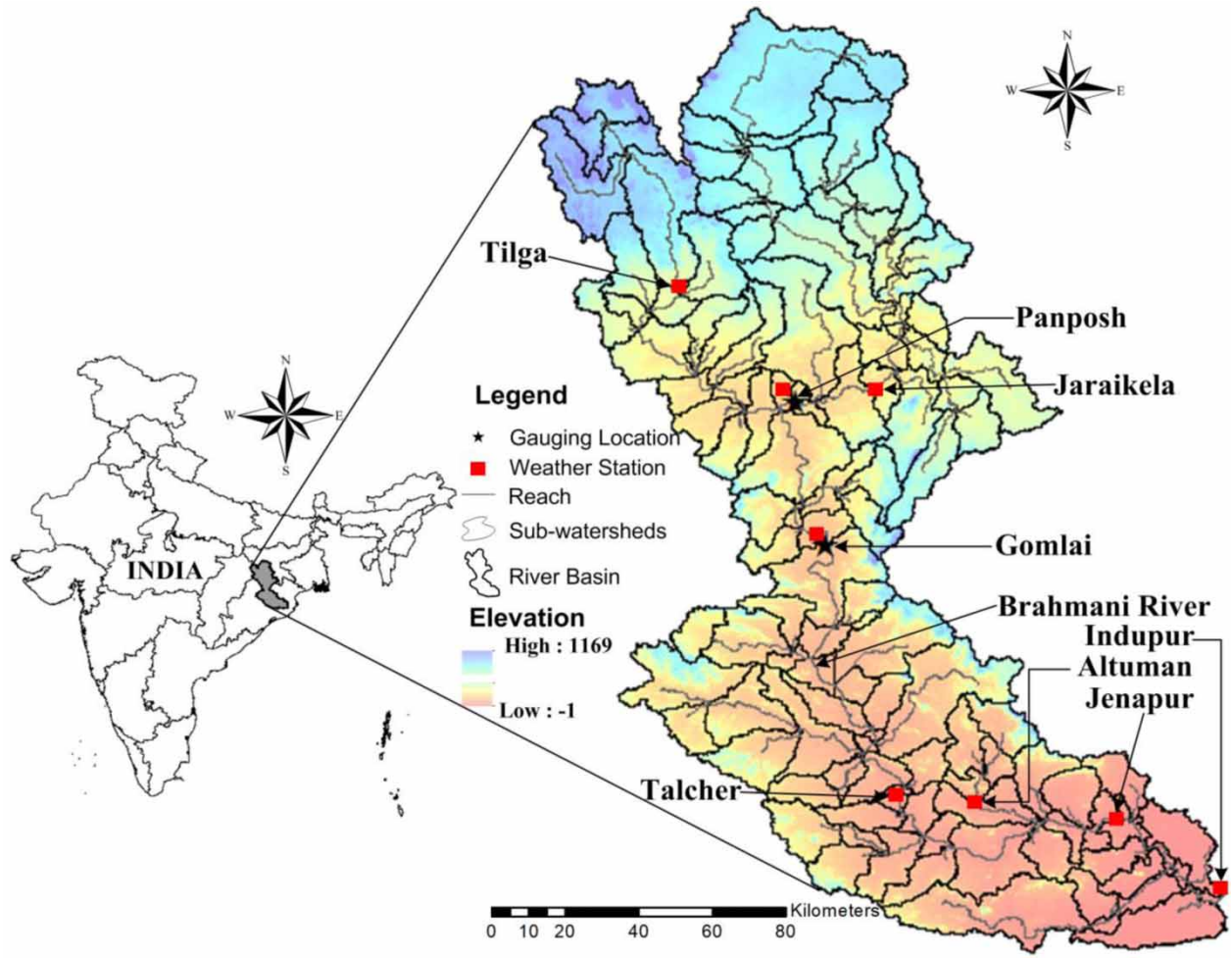

Figure 1 | Study area.

performed by two basic approaches: Soil Conservation Services (SCS) curve number (CN) approach (USDA Soil Conservation Service 1972) and the Green-Ampt infiltration method (Green & Ampt 1911). Moreover, the peak runoff rate is computed using the modified rational formula. SWAT performs the basic water balance to estimate the different flux components and given by Neitsch *et al.* (2011):

$$SW_t = SW_0 + \sum_{i=1}^{t} (R_{daily} - Q_{sur} - E_a - W_{seep} - Q_{gw}) \quad (1)$$

where SW_t is the final soil water content at period t (mm); SW_0 is the initial soil water content (mm); t is the time (no. of days); R_{daily} is the amount of precipitation on i^{th} day (mm); Q_{sur} is the amount of surface runoff on i^{th} day (mm); E_a is the amount of evapotranspiration on i^{th} day (mm); W_{seep} is the amount of water as recharge to groundwater from the soil profile on i^{th} day (mm); Q_{gw} is the amount of return flow on i^{th} day (mm).

In SWAT, various hydrological processes are characterized over multiple soil layers describing the role of complex sub-surface dynamics of catchment hydrology. The percolation loss is quantified by considering the types of crop grown and available soil water content in the subsequent soil layers. Under the saturated condition, the water moves downward to the underlying unsaturated soil layers and subsequently reaches the deep aquifer layers. The model individually computes evaporation from the soil and plant canopy surface. Soil water evaporation is an explicit function of the potential evapotranspiration (PET) and leaf

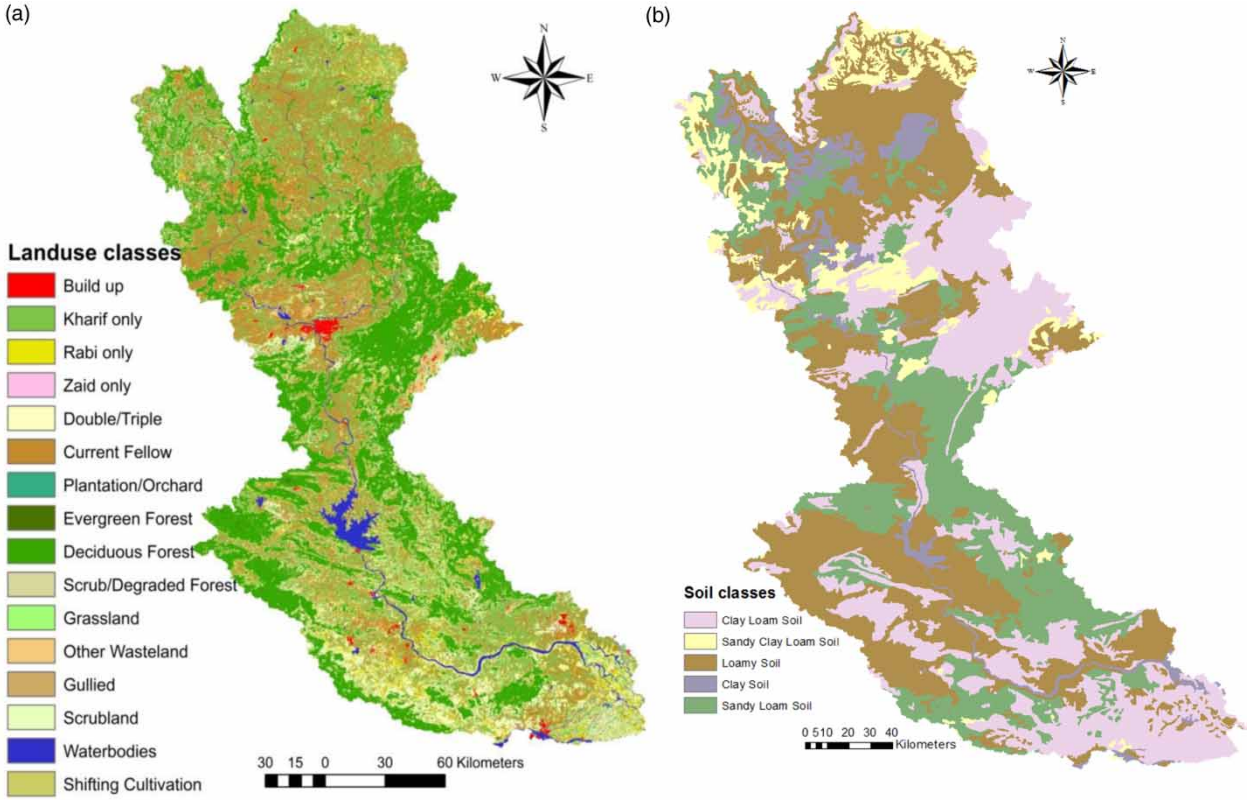

Figure 2 | (a) Land use land cover map; (b) soil map of the study river basin.

area index (LAI); that is, the ratio of plant leaf area to soil surface area. The PET of the catchment could be modelled with the inbuilt Penman-Monteith (Monteith 1965), Priestley–Taylor (Priestley & Taylor 1972), or Hargreaves (Hargreaves and Samani 1985) approach as per the input data availability; this study uses the Penman-Monteith approach to compute the PET. The catchment-scale sediment yield in SWAT is estimated by the modified universal soil loss equation (MUSLE), which was originally developed by Wischmeier and Smith (1978). The deposition and degradation of sediment processes occur simultaneously over the basin and are the basic driving units of sediment routing. Routing of sediments across the flow channel is carried out by using improved Bagnold's equation (Bagnold 1977).

Data sources

ASTER digital elevation model (DEM; Figure 1) of 30-m resolution was downloaded from the USGS EarthExplorer website (https://earthexplorer.usgs.gov/) and used for watershed delineation. Soil information was obtained from the National Bureau of Soil Survey and Land Use Planning (NBSS&LUP), Nagpur, Maharashtra. The soil physical properties required for model simulation include bulk density, saturated hydraulic conductivity, soil texture information, and available moisture content (AWC) given by:

$$\text{Available moisture content (AWC)} = \text{Field capacity (FC)} - \text{Wilting point (WP)} \quad (2)$$

Though the SWAT model can accommodate the soil information of ten layers as input, due to data unavailability, information of only two layers was used in this study. The land use data prepared by National Remote Sensing Centre (NRSC) at a spatial scale of 1:250,000 was utilized as input for HRU delineation. Observed weather data, precipitation (mm), minimum and maximum temperature (°C), wind speed (m/s), solar radiation (MJ/m^2), and relative

humidity (in percentage) for BRB at a daily time scale, was accessed from the Global Weather database for SWAT (https://globalweather.tamu.edu/). According to availability, eight weather stations were selected inside the basin and data for the period 1980–2013 was used in model simulation. Some missing information was generated through statistical simulation in SWAT by the SWAT-WGEN statistics. Daily streamflow data for the time period 1980–2013 was obtained from the Central Water Commission (CWC), Bhubaneswar for two surface flow gauging stations located at Panposh and Gomlai sub-basin and subsequently adopted in model calibration.

Model setup

Three basic GIS layers are required for running the SWAT model: DEM, land use/land cover, and soil map. These input layers were prepared in raster format or shape file format using the ERDAS IMAGINE 2014 and Arc GIS 10.1. The NRSC prepared map with 18 classes was resampled to a spatial resolution of 30 m (Figure 2(a)). For the preparation of the soil input layer, soil mapping units showing different soil classes were digitized (Figure 2(b)). Different soil properties were estimated from the FAO soil database and NBSS&LUP soil map for the individual mapping unit. The desired parameters were updated in the SWAT user soil database before the model simulation. All spatial data were projected to UTM 45N, datum WGS 1984 for the overlay of multiple spatial layers.

Individual sub-basin outlets and main catchment outlet were defined and 126 sub-basins were delineated. Land use and soil layers were reclassified as per the user-defined classes. Slope was obtained from the input DEM layer. Five slope classes were defined for the reclassification purpose. The HRU thresholds were defined as 10% for land use, 15% for soil, and 10% for slope classes to limit the number of HRUs and improve computational efficiency of the model. After overlaying these three layers with the predefined unique thresholds, 2,286 HRUs were generated. Six weather parameters, namely, precipitation, minimum and maximum temperature, solar radiation, wind speed, and relative humidity were provided as input on a daily basis. The data for the period 1980–2013 obtained from eight meteorological stations (i.e. Altuma, Gomlai, Panposh, Indupur, Jenapur, Talcher, Tilga, and Jarikela) were used as the inputs.

The model simulation was carried out for a period of 34 years, starting from 1 January 1980 to 31 December 2013. Three years of warm-up period was included for improving the simulation performance. To account for the heterogeneous distribution of rainfall over the study area, a skewed normal distribution pattern of rainfall was preferred. The parameterization approach was followed to account for spatial heterogeneity conceptually. Some model parameters, which could not be obtained directly from the present database, were estimated by the model calibration process. It facilitated understanding of the system behaviour as well as evaluating the applicability of the model (van Griensven *et al.* 2006). The Latin Hypercube Sampling and One-At-a-Time (LHS-OAT) technique was adopted to carry out the sensitivity analysis of model parameters using the results of simulation at different gauging stations. Sensitive parameters were identified and ranked accordingly. Initially, 22 parameters for runoff simulation were considered for sensitivity analysis. Pictorial representation of the adopted methodology for SWAT model simulation is shown in Figure 3.

Model calibration and validation

Instead of manual calibration, which is more time consuming and often fails to identify the inter-parameter sensitivity, an automatic calibration approach of SWAT-CUP tool (http://swat.tamu.edu/software/swat-cup/) was used. The Sequential Uncertainty Fitting (SUFI-2) algorithm was adopted for the calibration. An initial two years (1998–1999) was used as warm-up period and a period of ten years (2000–2009) was considered for model calibration. Out of the 22 parameters selected for sensitivity analysis results, only 15 parameters were chosen for carrying out the model calibration. Streamflow data at a daily scale of two gauging stations located at Panposh and Gomlai sub-basins were used as inputs for the calibration. For validation, a period of three years (2010–2012) was considered and the final fitted calibrated parameters were adopted for the same.

The several parameters related to streamflow were added to the calibration process; additional parameters to conceptualize the naturally occurring phenomena in the study area were also considered. The hydrological model,

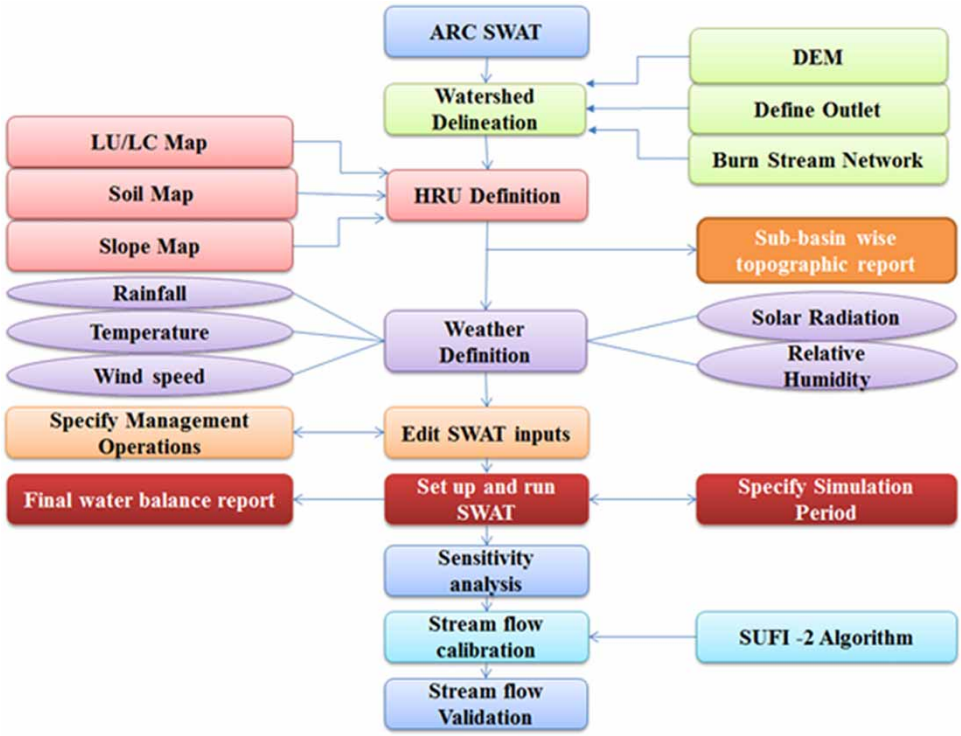

Figure 3 | Flow chart for SWAT model setup for simulation.

SWAT, was calibrated and validated using monthly average streamflow data. The streamflow calibrated model can be used for simulating sediment yields provided that the outcomes of rainfall and runoff meet the specified (Nash and Sutcliffe coefficient of efficiency (E_{NS}) >0.4 and $R^2 > 0.5$) criteria. The acceptable limit of percentage bias (PBIAS) was kept below 15% as defined by Moriasi *et al.* (2007).

Climate change impact assessment

The impact of climate change on hydrology and streamflow regime was quantified by using the calibrated and validated SWAT model for four different future climate scenarios assuming unchanged land use, soil type, and agricultural management practices for the study basin. The output of the HadGEM2-ES (Hadley Centre Global Environmental Model, Version 2, Earth System), which is an atmosphere-ocean general circulation model (AOGCM) with atmospheric resolution of N96 ($1.875° \times 1.25°$) with 38 vertical levels and an ocean resolution of 1° (increasing to ⅓° at the equator) and 40 vertical levels, was used for climate change impact analysis for the mid-century period (2050) (Collins *et al.* 2011). The future climate data for all four RCPs (i.e. 2.6, 4.5, 6.0, and 8.5) were analysed in this study. A low radiative forcing value, expected to reach a peak of 3.1 Wm^{-2} in the mid-21st century, and further decline to 2.6 Wm^{-2} by the end of the 21st century, is characterized by the RCP 2.6 scenario (Van Vuuren *et al.* 2011). The RCP 2.6 scenario can only be achieved through highly controlled greenhouse gas (GHG) emissions. In the case of RCP 4.5, a series of suitable adaptive measures might limit the radiative forcing value to 4.5 Wm^{-2} by the end of 2,100. RCP 8.5 being the highest emission scenario would raise the radiative forcing value to 8.5 Wm^{-2} by the end of 2,100 and tend to impact the ecosystem in the most adverse manner. The desired projected weather parameters were extracted for all 126 sub-basins at their respective centroid locations. The previously calibrated and validated SWAT model (base period) was further subjected to the future climate inputs for quantifying the desired hydrological fluxes.

Environmental flow assessment

Environmental flow (e-flow) is the minimum streamflow required to sustain the downstream river ecosystem (morphology, surface–groundwater interaction, groundwater recharge, aquatic life, and pollution by dilution, etc.). Out of numerous existing methods in the literature, the flow duration curve (FDC) approach was used to estimate e-flow. FDC is the graphical representation of river discharge (magnitude) in P^{th} percentile of daily, monthly, annually, or any other time interval versus exceedance probability (frequency). An integrated approach of 1-day, 7-days, and 30-days mean is generally used for developing the FDCs (Efstratiadis *et al.* 2014; Sahoo *et al.* 2016). In this study, 30-days mean was chosen for developing the FDC for the BRB. Q_{95} and Q_{90} are treated as the low flow index for estimating environmental flow (Sahoo *et al.* 2016), whereas (Q_{50}/Q_{90}) represents the variability of low-flow discharges. Ratio (Q_{90}/Q_{50}) can be interpreted as an index representing the contribution of groundwater sources towards the streamflow, excluding the effects of catchment area, and Q_{95} is rated as the best index that corresponds to minimum ecological flow requirement (Jha *et al.* 2008). Streamflow was calculated at Q_{50}, Q_{90}, and Q_{95} percentile for identifying the e-flow under present and future climate change scenarios.

Vulnerability assessment

For identification of vulnerable sub-basins in order to propose effective conservation practices, it is necessary to recognize those sub-basins with a higher peak and average runoff and sediment yield. Sub-basin-wise average runoff and sediment yield value were normalized in the range from 0 to 1, to nullify the effect of multiple units as suggested by Jeong & Kim (2005). Equal weight (0.5) was assigned to both runoff and sediment yield for assessment of their combined effect for identifying the critical zone, represented by the vulnerability index value. Five vulnerable classes were categorized, slight, low, moderate, high, and extreme (Table 1), to classify the erosion-prone regions.

Goodness of fit assessment

The calibrated parameters were updated in the raw model database and subsequently the simulated outputs were compared with the observed streamflow values for goodness of fit assessment. The extent of statistical significance between simulated and observed values was assessed using three popular statistical indicators: E_{NS} (Nash & Sutcliffe 1970), one of the popular objective functions used in hydrology studies (Willmott *et al.* 2015); coefficient of determination (R^2); and *PBIAS*. The mathematical expression of E_{NS}, R^2, and *PBIAS* are presented in Equations (3)–(5), respectively.

Table 1 | Criteria for identification of critical sub-basins

Vulnerability index	Vulnerability classes
<0.16	Slight
0.16–0.33	Low
0.33–0.49	Moderate
0.49–0.65	High
>0.65	Extreme

$$E_{NS} = 1 - \frac{\sum_{i=1}^{n}(O_i - P_i)^2}{\sum_{i=1}^{n}(O_i - O')^2} \tag{3}$$

Moreover, co-linearity between simulated and observed values was interpreted using the R^2, and it ranges from −1 to 1.

$$R^2 = \left\{ \frac{\left(\sum_{i=1}^{n}(O_i - O')(P_i - P')\right)^2}{\sum_{i=1}^{n}(O_i - O')^2 \sum_{i=1}^{n}(P_i - P')^2} \right\} \tag{4}$$

$$PBIAS = \frac{\sum_{i=1}^{n}(O_i - P_i)}{\sum_{i=1}^{n} O_i} \times 100 \tag{5}$$

where n is total number of observed data, O_i and P_i are observed and simulated data at time i, O' and P' are the mean of observed and simulated data. The nearer the value of E_{NS} and R^2 to 1, the better the model tends to perform in modelling and capturing the dynamics. E_{NS} generally lies between $-\infty$ and 1; more positive values

indicate that the model reproduced the observed values with utmost accuracy both spatially and temporally. However, a PBIAS value between −25 and +25% is treated as acceptable in hydrological modelling studies.

RESULTS

Sensitivity analysis

Model calibration and validation were performed on a monthly time scale for the Panposh and Gomlai sub-watersheds for the years 2000–2009. Sensitivity analysis results of the parameters and the calibrated values of streamflow parameters of the ArcSWAT model are presented in Table 2. Sensitivity analysis operation was performed for both the calibration and warm-up periods. Four iterations were performed in the SWAT-CUP. Out of 22 parameters, ten were found most sensitive during the calibration processes and were ranked according to the objective function value; that is, *P*-value and absolute *t*-stat between observed and simulated streamflow values. Streamflow was found to be impinged by both surface water and groundwater parameters of the study basin (Table 2) indicating diverse hydrological variability in the study area.

The most important baseflow calibration parameter is baseflow alpha factor (ALPHA_BF), which explains the contribution of groundwater flow to variation in the recharge.

Table 2 | Model parameters range and fitted value during calibration period

		Bound		Auto-calibration result	
Parameter	Rank	Lower	Upper	Fitting value	Method
RCHRG_DP	1	0.03	0.5	0.15	Replace
SOL_K	2	0.28	0.65	0.60	Relative
CH_N2	3	0.02	0.2	0.02	Replace
SOL_AWC	4	−0.12	0.12	−0.02	Relative
ALPHA_BF	5	0.2	1	0.92	Replace
SLSUBBSN	6	0.06	0.14	0.08	Relative
ALPHA_BNK	7	0.28	0.52	0.33	Replace
GW_SPYLD	8	0.16	0.28	0.23	Replace
GW_DELAY	9	0.87	1.79	1.12	Replace
GWQMN	10	2,878	4,660	4,234	Replace

ALPHA_BF also bears a direct relation with another groundwater calibration parameter, groundwater recession constant. A higher value of these two parameters indicates a quick response to groundwater recharge in the basin. Due to lack of knowledge regarding the basin hydrology, the complete calibration ranges of ALPHA_BF (i.e. 0–1) was considered in this study. The Manning's *n*-value for main channel (CH_N2) was found to be the third most sensitive parameter indicating variable topography of the basin. Sub-basin slope parameter (SLSUBBSN) was another sensitive parameter that affects the flow properties to a greater extent. The SOL_K, an indicator of ease of water movement inside the sub-surface soil strata was also a sensitive parameter. High runoff may be attributed to the existence of some seasonal (intermittent) tributaries which contribute flow to the main river. A moderate value of river-bank flow recession constant (ALPHA_BNK) suggests the movement of water between some regions of bank storage and adjacent unsaturated zones due to severe water stress. The higher GW_DELAY value indicates the increased resting time of water over the soil surface resulting in a significant increase in surface runoff. The reduced GW_SPYLD value also would have added the higher value of streamflow. The sensitivity of various parameters suggested that the surface runoff characteristics of the BRB are affected by both surface and sub-surface flow control parameters. This could be due to joining of different intermittent streams from different locations to the main stream.

Uncertainty analysis

The magnitude of P-factor and R-factor were found to be different for different gauging locations (Table 3). During the calibration process, the value of P-factor and R-factor at two different gauging stations was slightly higher than 0.5 which indicates the close agreement between observed and simulated values. The 95% prediction uncertainty (95-PPU) band is relatively narrower as suggested by the R-factor value. During the validation period, P-factor was 0.58 for both stations and R-factor was 0.20 and 0.26 for the respective gauging stations Panposh and Gomlai. The higher value of the P-factor compared with the calibration period and R-factor close to 0 indicate that validation was adequate. The parameters used in calibration and validation

Table 3 | Statistics for runoff simulation during calibration and validation periods

		Calibration					Validation				
Gauging location	**Sub-basin number**	**P-factor**	**R-factor**	E_{NS}	R^2	**PBIAS**	**P-factor**	**R-factor**	E_{NS}	R^2	**PBIAS**
Panposh	54	0.49	0.50	0.54	0.51	13.7	0.58	0.20	0.44	0.71	9.2
Gomlai	68	0.48	0.51	0.52	0.52	11.7	0.58	0.26	0.55	0.72	7.4

were obtained by the regional approach of river flow prediction at the gauging stations. Therefore, they were not affected by any water storage structures or reservoirs located in the upstream. The unavailability of consistent data of reservoir inflow-outflow at a daily timescale for simulation of runoff was a constraint and main reason for uncertainty.

Model calibration and validation

The initial simulation showed an E_{NS} value of 0.12 and R^2 of 0.26 at Panposh and E_{NS} 0.06 and R^2 0.23 at Gomlai between simulated and observed streamflow. Successive simulations and subsequent alteration in the parameter values resulted in significant improvement in streamflow prediction. The final calibration and validation statistics are presented in Table 3. The comparison between daily observed and simulated streamflow at both the gauging stations, Panposh and Gomlai, are shown in Figures 4 and 5, respectively.

During the earlier years (2000 and 2001), the model continuously underestimated the observed streamflow. With the advancement of the calibration process, the same trend was also observed in August 2005 and 2006. This may be due to the high amount of rainfall in August which could not be adequately addressed by the model. Towards the end of the calibration period, the model was able to simulate the observed values with reasonable accuracy (Figure 4). During the calibration process, the model did not overestimate the observed values for a single period, indicating the groundwater contribution towards the streamflow generation process. Similar trends were also observed during the validation period of BRB. The close agreement between observed and simulated streamflow during the validation period indicated improved model performance, consistency, and capability in producing good output with future changing climatic scenarios.

Climate change impact assessment

Projected precipitation and temperature

The variation in rainfall is found to be maximum in RCP 8.5, whereas a marginal increase is expected under RCP 2.6 and RCP 4.5 with respect to the base period rainfall of 1,644 mm. The maximum increase in rainfall is projected during July and August for all the RCP scenarios. For all the RCPs, rainfall increases over the space, except a few areas where a significant decrease in rainfall was observed. About 60% of total basin area would experience 5–10% increased rainfall across all the RCPs, whereas about 30% of the area would experience 10–15% increase in rainfall, except for RCP 4.5. In RCP 8.5, an average rainfall of 450 mm might occur during August. Increase in projected temperature over BRB indicated that RCP 8.5 would correspond to an extreme climate scenario. The temperature might go beyond 45 °C with an increase of 3.7 °C in minimum temperature and 2.9 °C in maximum temperature during April. The spatio-temporal analysis shows a gradually increasing pattern of temperature for all four RCPs. The Mann-Kendall trend tests (parametric trend analysis approach) statistics indicated an average increase in temperature at the rate of 0.3 °C per year in the projected future scenarios compared with the baseline scenario.

Alteration in flow duration curve

FDC indicates a substantial and significant alteration in flow regime under projected climate compared with the base period. A relatively small but significant difference is also observed among different RCPs, except between RCP 4.5 and 6.0. The maximum increase in the streamflow is under RCP 8.5 (Figure 6). Q_{50} is likely to be doubled by mid-century compared with the base period, whereas a

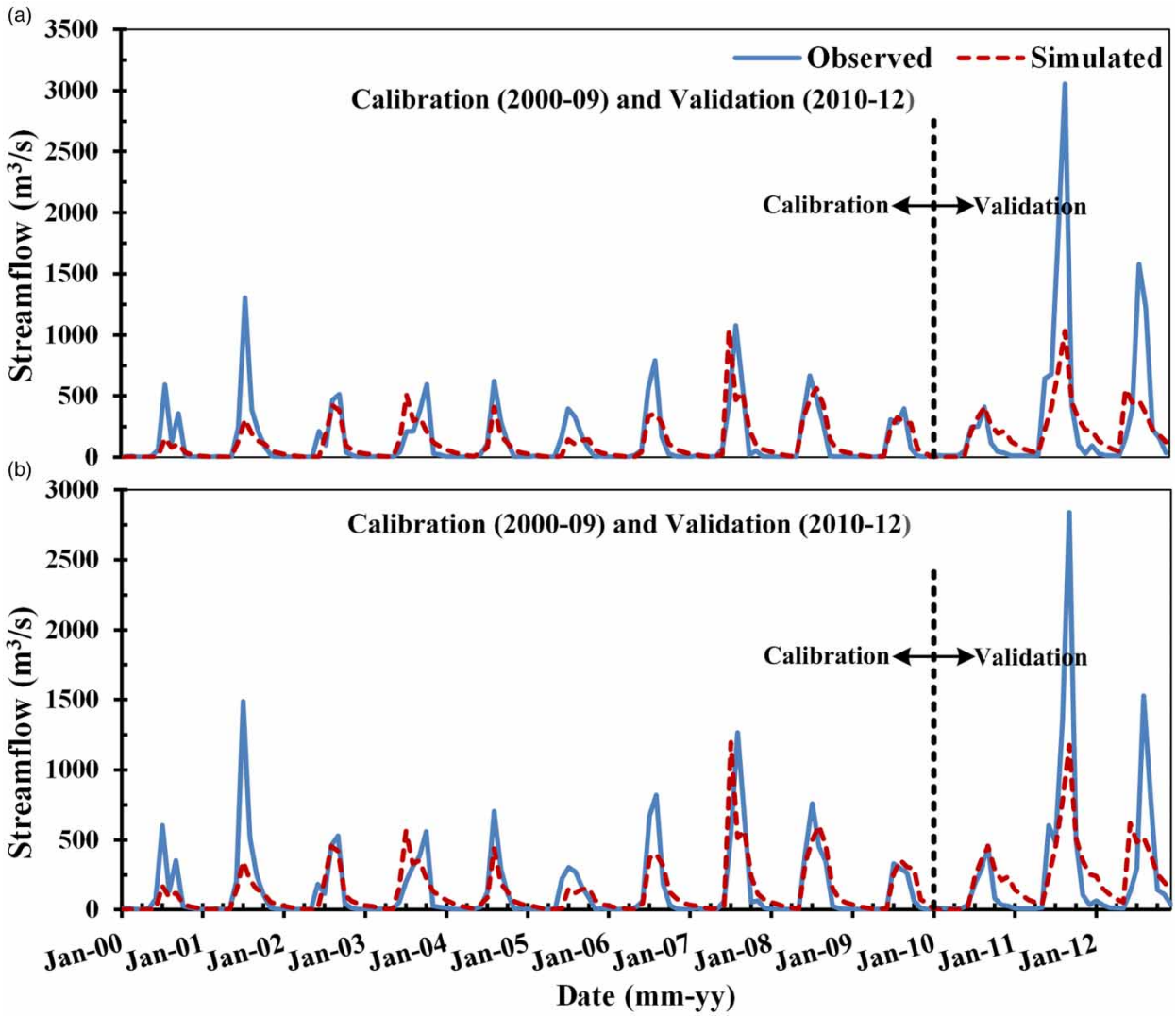

Figure 4 | Time series plot of measured and predicted monthly runoff at (a) Panposh and (b) Gomlai during calibration and validation periods.

ten-fold increase in Q_{90} is predicted for the same period (Table 4). The e-flow is necessary for maintaining a balanced ecosystem and can be easily fulfilled with such increased streamflow scenarios in the future climate. The increased water availability in streams under future climate may be managed to fulfil various requirements, such as irrigation water supply, hydropower plant projects, and ongoing urbanization. However, to actualize the benefit of increased water flow, existing water storage structures or reservoirs need to be upgraded and some new water conservation structures need to be constructed in the BRB.

Sub-basin-wise variation in streamflow and sediment yield

To conserve soil and water by implementing best management practices (BMPs), it is essential to identify and prioritize the critical sub-basins. The impact of climate change on hydrology was quantified by comparing the calibrated SWAT model outputs of base periods (1970–1999) and mid-century period, 2050. The preliminary assumption of this study was that land use, soil type, and agricultural practices remained unchanged in the study area for the

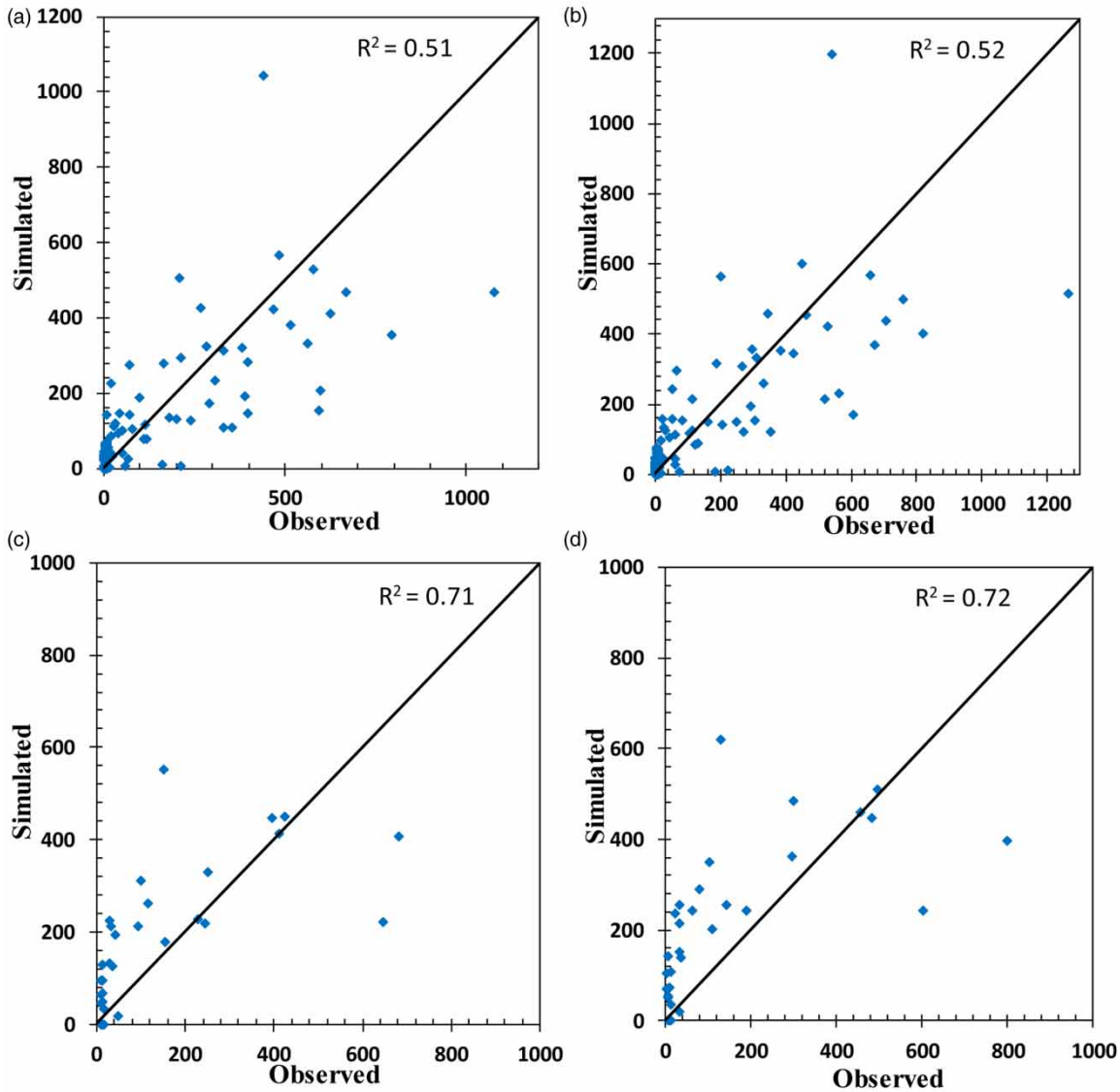

Figure 5 | Scatter plots of monthly observed and simulated streamflow during calibration at (a) Panposh and (b) Gomlai; and for validation (c) Panposh and (d) Gomlai.

analysis period, and the change occurs only due to the change in climatic input variables. In the present study, climate data of the Intergovernmental Panel on Climate Change (IPCC), AR-5 were used. Data of the four RCPs (2.6, 4.5, 6.0, and 8.5) for the mid-century were given as input to the previously calibrated model. The resulting changes in the streamflow values of the BRB are in the order of 20.86, 11.29, 4.45, and 37.94% under RCP 2.6, 4.5, 6.0, and 8.5, respectively, while for sediment yield the percentage increase becomes 23.34, 10.53, 2.45, and 27.62% under RCP 2.6, 4.5, 6.0, and 8.5, respectively. The contrasting results for the streamflow for RCP 6.0 could be attributed to the high evapotranspiration loss as a consequence of highest temperature increase (5.51 °C), subsequently lowering the streamflow component of the water balance. Certainly, the lowest increase in streamflow caused reduced sediment yield from the BRB in the RCP 6.0 scenario. These results are expressed as the sub-basin-wise percentage variations in runoff and sediment yield, respectively for each RCP (Figures 7 and 8). As per the

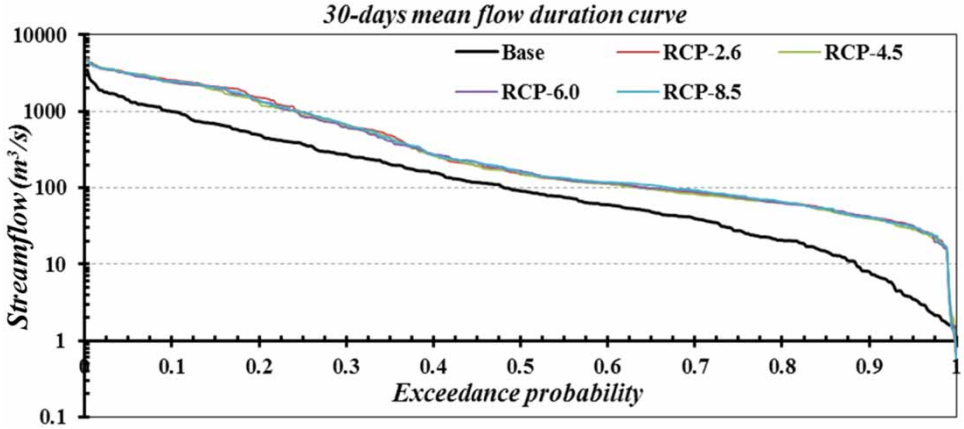

Figure 6 | Comparison of FDC of 30-days mean streamflow for present and future climate change scenarios.

Table 4 | Environmental flow (m^3/s) variation in base period and climate change scenarios

	Q_{50}	Q_{75}	Q_{90}	Q_{95}
Base period	82.43	22.7	4.462	1.69
2050-RCP 2.6	148.70	73.14	39.69	28.52
2050-RCP 4.5	149.8	71.28	39.32	28.23
2050-RCP 6.0	162.80	73.67	40.89	30.58
2050-RCP 8.5	157.40	77.57	40.34	30.07

value of proposed vulnerability using an equal weight approach for runoff and sediment yield, sub-basins were categorized into five vulnerability classes such as slight, low, moderate, high, and extreme. The areas under five vulnerability classes were calculated sub-basin-wise for both present and future climate change scenarios and are presented in Table 5. During the base period, the area under extreme and high vulnerability classes were 3.5% and no substantial change is found under projected climate change scenarios.

Identification of vulnerable area

The highest increase in area is indicated under the moderately vulnerable class followed by the highly vulnerable class. The area under the slight and low vulnerability classes decreased from the initial value of 24.5–15.8% and 44.9–29.8%, respectively, in the future climates. The result indicates an increase in overall soil erosion potential for the BRB under projected climate scenarios.

During the base period, five critical sub-basins (sub-basin number 1, 2, 16, 17, and 22) cover 3.5% of the total basin area. Sub-basins 1 and 2 are largely encompassed under village area and the majority of the land portion is covered with agricultural lands. About 48% of the area (12,719.8 ha) remains fallow throughout the year. However, the fallow land may be covered with crops due to altered rainfall patterns which is indicative of the improved hydrologic scenario in the future time period (Figure 7). More than 50% of land area is situated on slope ranges of 8–33%. This land topography also corroborates the high vulnerability of these two sub-basins. In case of sub-basin 16, 17, and 22, increased rainfall and high slope are favourable for the erosion and transportation of soil particles. Approximately 30% of basin area comes under the moderate to extreme vulnerability class and needs priority attention. Only 5.5% of the area is categorized under severe and high erosion-prone zone (Figure 9). Spatial heterogeneity regarding projected climate change and hydrological alterations in BRB is also corroborated from the predicted reduction in the vulnerability of some patches against the overall increased vulnerability.

In the projected climate condition, around 55% of the total area is under the moderate to extremely vulnerable class which is almost double that of the base scenario. Though no considerable change is observed in case of severe erosion-prone areas, an increase of around 12% is observed in the case of high erosion-prone areas. The percentage of slight erosion-prone areas reduced from an initial value of 24.5%–15.7%.

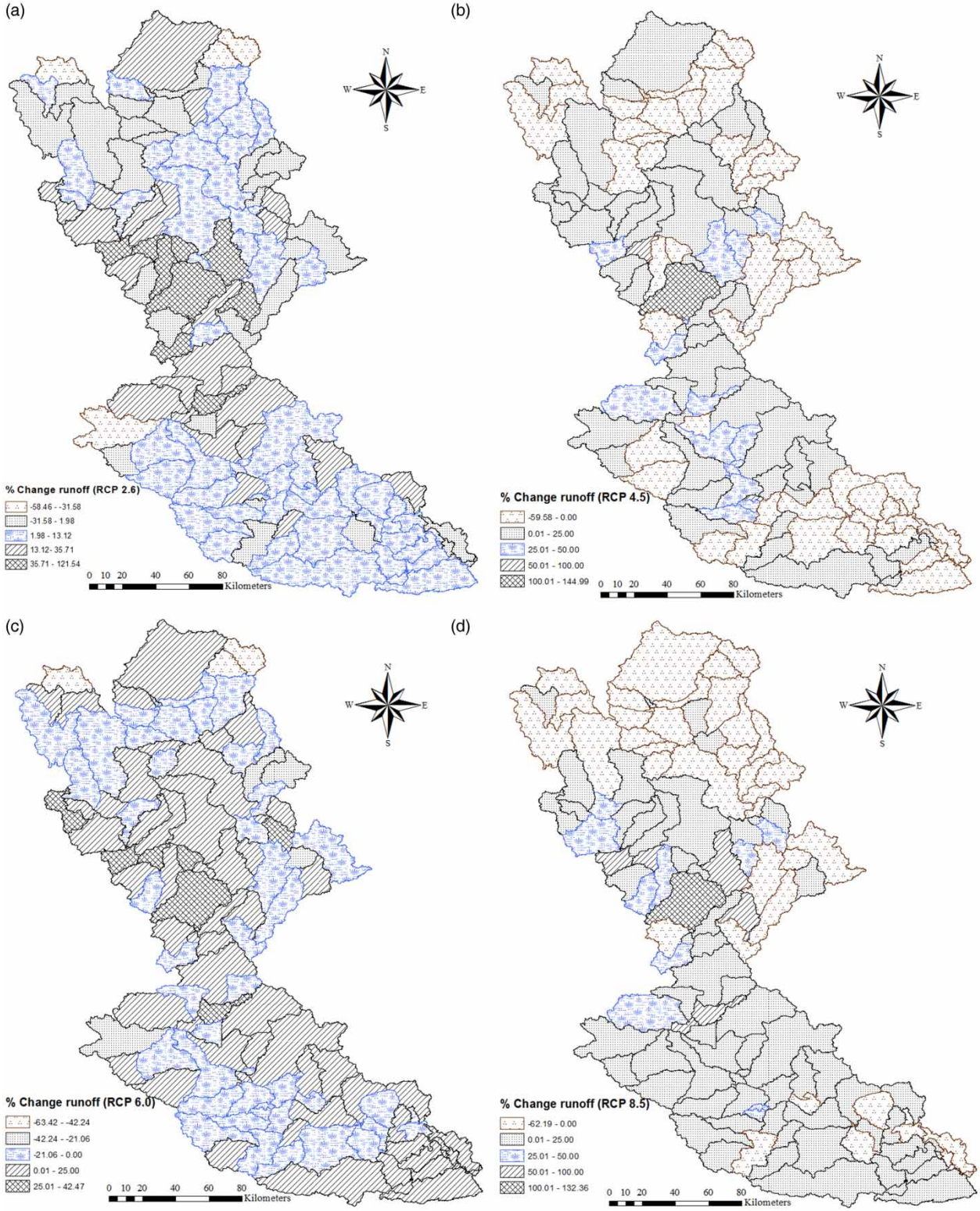

Figure 7 | Sub-basin-wise percentage changes in runoff with respect to base period for the four scenarios (a) RCP 2.6; (b) RCP 4.5; (c) RCP 6.0; and (d) RCP 8.5 for 2050.

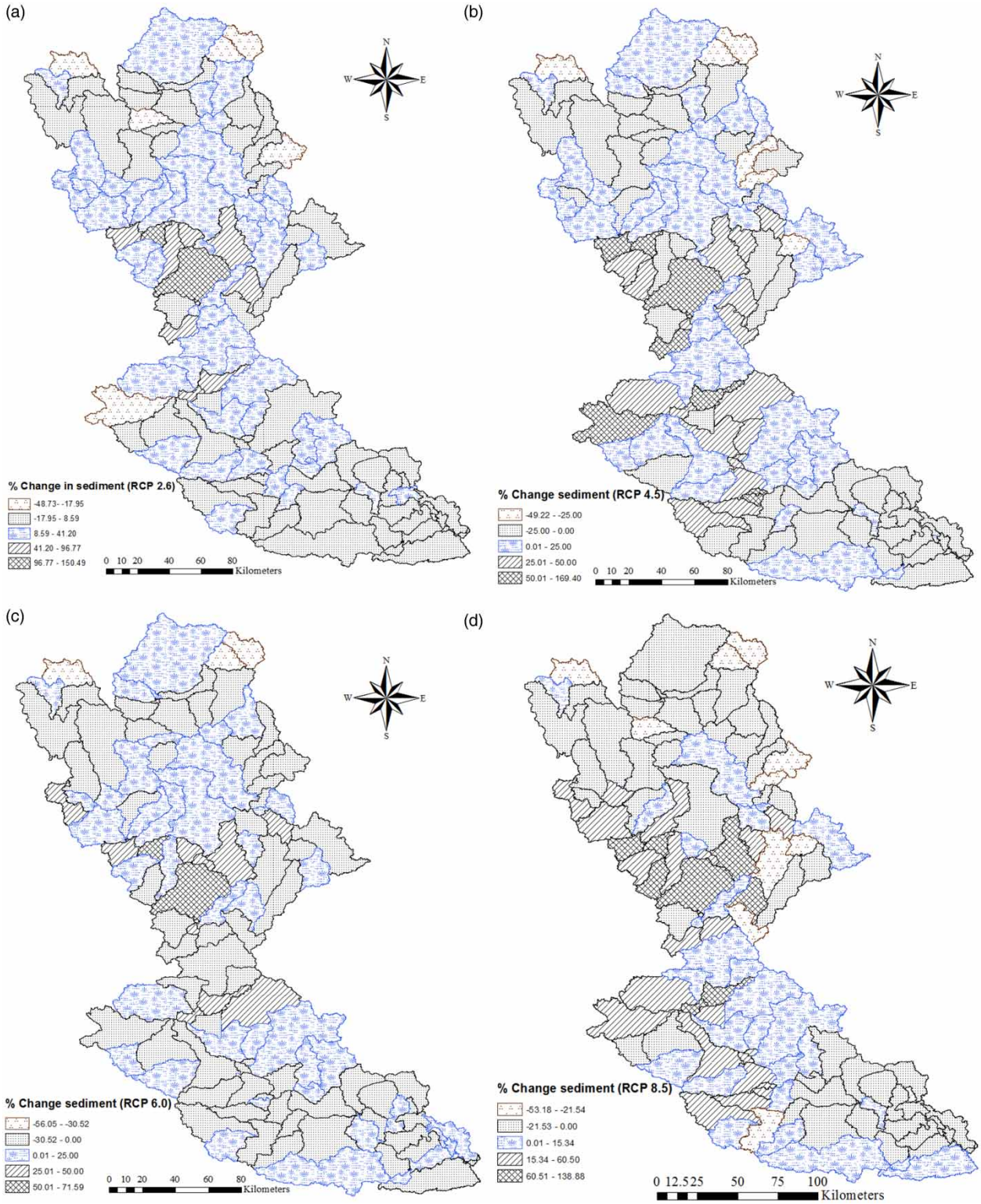

Figure 8 | Sub-basin-wise percentage changes in sediment yield with respect to base period for the four scenarios (a) RCP 2.6; (b) RCP 4.5; (c) RCP 6.0; and (d) RCP 8.5 for 2050.

Table 5 | Vulnerable classes and percentage area under present and climate change scenarios

Vulnerable classes	Area (%) during base period	Area (%) under changing climate scenario
Slight	24.49	15.74
Low	44.87	29.79
Moderate	25.25	36.66
High	1.90	13.8
Extreme	3.48	3.65

In the projected future climate scenario, maximum soil erosion is observed in the case of sub-basin numbers 16, 20, 22, 104, and 118. This may be attributed to long patches of fallow land in the two sides of Brahmani River and undulating topography resulting in high levels of soil erosion under increased flow in sub-basin 16. Hilly topography of sub-basin number 20 under increased precipitation makes the sub-basin extremely vulnerable. Hence, it is classified under severe erosion-prone area. High rainfall (1,512 mm) projected in sub-basin 22 during the period 2050–2079 along with high slope (15–33%) explains the high vulnerability of the concerned region. Sub-basins (104 and 118) situated close to the outlet of Brahmani River basin are subjected to high flow velocity of the main stream. Precipitation in these areas is also projected to increase (about 1,650 mm), which explains their inclusion under severe soil erosion-prone zones in future climate scenarios.

DISCUSSION

Flux variation under changing climate scenarios

The results of the present study are in line with the results reported from similar climatic regions. A study carried out by Pandey *et al.* (2017) over the Godavari River basin, India, which lies in a tropical region, found an increase in the magnitude of various hydrological fluxes in both A2 and B2 scenarios. The increase in water yield during May

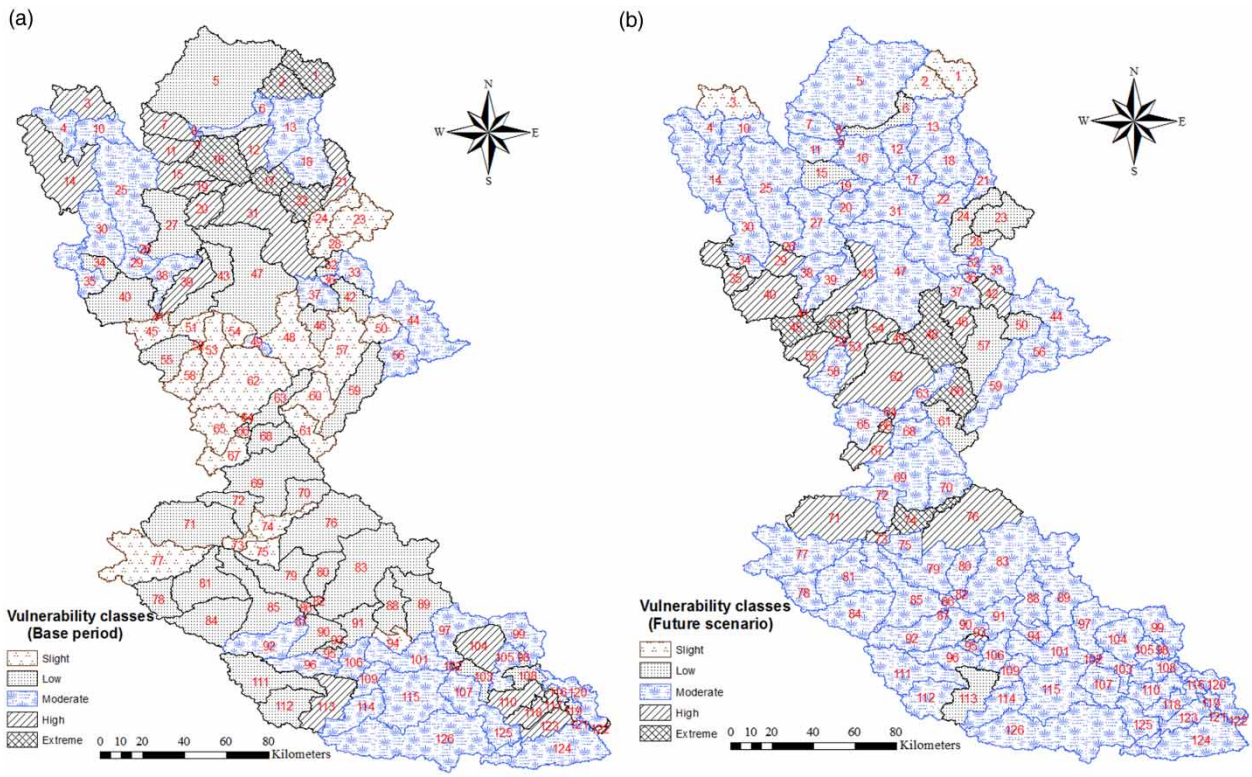

Figure 9 | Sub-basin-wise vulnerability classes for the period (a) 1970–1999 and (b) 2050–2079.

was nearly 16%. These results are found to be in line with the results of the present study showing increased streamflow of 0–30%. The average increase in sediment yield of 18% over BRB is comparable with results reported by Plangoen *et al.* (2013) over a tropical watershed of northern Thailand. The HadCM3 model indicated an increase in soil erosion by 14% with 4% change in rainfall magnitude over the region.

Contrasting results are also reported from a different type of climatic region. Reduction in runoff by 39.2 and 41.25%, in A2 and B2 scenarios, respectively, has been reported from the humid region (Perazzoli *et al.* 2012). Net alteration in radiation results in an increase in precipitation round the year, and subsequently the forest canopy gets denser and controls the average streamflow to a greater extent (Graham *et al.* 1990). The study over the tropical region and humid region confirms that in future the pattern of streamflow is a region/climate-specific phenomenon and largely depends on the variation in meteorological parameters. In the case of humid regions, a decrease in precipitation is reflected in the reduced streamflow, whereas the opposite trend is observed in tropical regions including the present study.

Effect of flux alteration over different water resource sectors

Climate change impact and subsequent alteration in hydrological fluxes has significant implications for the sustainable planning of water resources. As runoff and sediment yield are the two important concerns of this study, an attempt has been made to identify the soil erosion-prone areas under changing climate scenarios. BRB is primarily an agriculture-dominant river basin, with more than 40% of the area covered with *Kharif* and *Rabi* crops. Apart from agriculture, BRB plays a crucial role in electricity production as it houses one of the major hydroelectric power plants at Rengali reservoir. The hydroelectric power plant has an installed capacity of 250 MW. It also assists two basic water resource management strategies by protecting an area of around 2,600 km^2 from flood hazard and simultaneously providing irrigation to 270,000 hectares in the downstream area. At present, the hydroelectric power plant operates based on the run-of-the-river policy (ROR), which indicates that the magnitude of hydropower generation is directly proportional to reservoir inflow volume. The analysis of climate change impact in subbasin 62 indicated that Rengali reservoir and hydroelectric power plant would experience more than 100% increase in discharge under all RCP scenarios of 2050. This alarming situation would need a plan and additional infrastructure for additional flow management of Rengali reservoir. The increased reservoir inflow may cause severe siltation problems in the reservoir, resulting in considerable reduction in storage volume and elevated peak discharge. This challenging situation offers an opportunity for increasing water availability if the information generated is used for pre-event policy planning for sustainable management.

The flow duration curve prepared for both base period and future scenarios of all RCPs indicate a significant variation between these two projections. In general, Q_{50} corresponds to the flow required to maintain hydroelectric power plant operations, which is predicted to increase by 50% in future projections. This brings a very good opportunity for hydroelectric power generation in the mid-century period. However, increased water availability for hydropower generation in future projections raises a serious concern about maintaining the capacity of the hydroelectric power plant. Similarly, the Q_{75} value in FDC corresponds to the irrigation water supply to downstream areas for maintaining crop water requirement throughout the growing period. This value may increase three-fold under the future scenario, which may have a positive impact on crop growth and yield enhancement.

From the water availability aspect over BRB, an improved situation is expected in the mid-century. However, the real problem arises when erosion-prone areas come into the picture. Though no appreciable change in the area susceptible to severe erosion is predicted, there is a likelihood of an increase in moderate and high erosion-prone areas. If not attended properly, the increased erosion potential may negate the positive effect of increased water availability for crop production. Due to the adverse soil erosion potential in the mid-21st century, a contradictory scenario would be created when the benefit of a large amount of available water for irrigation would not be actualized to a satisfactory extent due to the reduced availability of fertile land.

As described earlier, the BRB is going to be an industrial hub in the near future, causing a significant reduction of the

existing crop lands. The rapid industrialization may further aggravate population increase to greater extent. Under such a contradictory scenario, the need to maintain the balance between food demand and existing crop land is inevitable. Therefore, to increase crop productivity in the BRB, the fallow land, wasteland, and eroded land need to be treated properly before their use for agriculture. The outcomes of the future climatic projections over BRB revealed that the moderate and highly vulnerable areas may experience considerable increase over that of base period. Hence, best management practices can be implemented in the identified critical sub-basins in the future climate context over BRB, such as bunding, terracing, and contour farming, so that the crop yield and available agriculture land can be optimized. Moreover, the identified extreme erosion-prone regions can be managed properly so that soil erosion can be reduced dramatically. The conversion of waste lands and fallow lands to agriculture lands and reduced erosion will alleviate the flood hazard and subsequently, the reservoir efficiency in fulfilling the water demand may be further improved.

SWAT has been extensively used in water balance studies, but the erosion perspective attempted in this study using recently available climate change projection (IPCC AR5) and the contribution of both streamflow and sediment yield in erosion-prone area identification is the new addition. The attempt to develop FDC using recently available climate change projections (AR5), using the SWAT model for future climate projections to assess the water availability and subsequent allocation to different water resource sectors to maintain minimum ecological flow is of its own kind in the BRB. A similar approach can be extended to other river basins worldwide irrespective of region and climate. The study highlighted the following useful points that can improve the modelling efficiency and accuracy to a greater extent in basin scale water resources planning. Selection of appropriate climate model and RCP scenarios has substantial implications for the assessment of water resources. Moreover, the hydrological modelling of catchments with a wide nexus of agriculture, flood, drought, and hydropower generation necessitates selection of appropriate hydrological models for a more realistic assessment of water resources in future climate change scenarios, and subsequent planning processes.

CONCLUSION

The hydrology of BRB was quantified for the baseline period (1970–1999) as well as for future climate (mid-century, 2050). The SWAT model could be successfully used for simulation of BRB hydrology. Integration with the SWAT-CUP tool and SUFI-2 algorithm for calibration and validation was found to be very effective. A good agreement between observed and simulated streamflow during calibration and validation proves the applicability of the SWAT model at river basin-scale under a limited data availability scenario. Bias-corrected outputs of GCM (HadGEM2-ES) were used to assess the impact of changes on runoff and sediment yield. The variability of climatic factors is found to be at a maximum during the RCP 8.5 scenario for the mid-century.

Overall, runoff and soil loss are predicted to increase under future climate change conditions. However, a decrease in runoff and sediment loss is indicated from some patches in upper catchments of the BRB. Increase in runoff and sediment yield indicated from mid- and lower catchments may be attributed to increased rainfall magnitude, altered rainfall pattern (Figure 6), interaction with topography, and land use under future climate. An approximate ten-fold increase in environmental flow (Q_{90}) is expected under projected climate scenarios. The increased flow can be managed to fulfil the ever-increasing demand of various sectors and can be of great support for ongoing urbanization. The area under moderate and high vulnerability classes is likely to increase from 25 to 37% and 2 to 14%, respectively, by the mid-century. A substantial area under the low and slightly vulnerable classes is likely to be converted to the moderate and highly vulnerable classes under the changed climate. The area in need of soil and water conservation treatment is likely to double (55% of total area) under future climate change context. The critical sub-basins identified in this study can be taken up as a priority for introducing best management practices (BMPs) to sustain agricultural productivity and judicious water resource management. Conclusively, the threat to hydroelectric plants for power production is imminent due to climate change scenarios across all the RCPs in BRB.

This study provides a generalized framework for the identification of the vulnerable areas in a watershed/river

basin in the context of climate change. The outcomes of this research would act as a guiding tool for policy makers to identify the locations where implementation of suitable best management practices (BMPs) may alleviate future adverse conditions to a greater extent. In future studies, more complex frameworks can be integrated with the existing approach to identify the vulnerable regions in both climate change and land use/land cover change scenarios.

ACKNOWLEDGEMENTS

The authors would like to acknowledge the generosity of the ICAR-Indian Institute of Soil and Water Conservation, Dehradun and NICRA project for providing resources to carry out this study. The hydro-meteorological data provided by the CWC and Indian Meteorological Department (IMD), Bhubaneswar is highly appreciated. The fellowship provided by the ICAR, New Delhi to the first author during the M. Tech degree programme is duly acknowledged. On behalf of all authors, the corresponding author states that there is no conflict of interest.

REFERENCES

Abbott, M. B., Bathurst, J. C., Cunge, J. A., O'Connell, P. E. & Rasmussen, J. 1986 An introduction to the European Hydrologic System-Systeme Hydrologique Europeen, SHE, 1: History and philosophy of a physically-based, distributed modeling system. *Journal of Hydrology* **87**, 45–59.

Adhikary, P. P., Sena, D. R., Dash, C. J., Mandal, U., Nanda, S., Madhu, M., Sahoo, D. C. & Mishra, P. K. 2019 Effect of calibration and validation decisions on streamflow modeling for a heterogeneous and low runoff-producing river basin in India. *Journal of Hydrologic Engineering* **24** (7), 1–12.

Arnold, J. G., Srinivasan, R., Muttiah, R. S. & Williams, J. R. 1998 Large area hydrologic modeling and assessment – part I: model development. *Journal of the American Water Resources Association (JAWRA)* **34** (1), 73–89.

Bagnold, R. A. 1977 Bedload transport in natural rivers. *Water Resources Research* **13**, 303–312.

Burnash, R. J. C., Ferral, R. L. & McGuire, R. A. 1973 *A Generalized Streamflow Simulation System – Conceptual Modeling for Digital Computers*. Technical Report, Joint Federal State River Forecast Center, US National Weather Service and California Department of Water Resources, Sacramento, California.

Chen, T., Niu, R., Li, P., Zhang, L. & Du, B. 2011 Regional soil erosion risk mapping using RUSLE, GIS, and remote sensing: a case study in Miyun watershed, North China. *Environment and Earth Science International* **63**, 533–541.

Chow, V. T., Maidment, D. R. & Mays, L. W. 1988 *Applied Hydrology*. McGraw-Hill Inc, New York, USA.

Collins, W. J., Bellouin, N., Doutriaux, B. M., Gedney, N., Halloran, P., Hinton, T., Hughes, J., Jones, C. D., Joshi, M., Liddicoat, S., Martin, G. O., Connor, F., Rae, J., Senior, C., Sitch, S., Totterdell, I., Wiltshire, A. & Woodward, S. 2011 Development and evaluation of an earth-system model HadGEM2. *Geoscientific Model Development Discussions* **4**, 997–1062.

Crawford, N. H. & Burges, S. J. 2004 History of the stanford watershed model. *Water Resources Impact* **6** (2), 3–5.

Dash, S. S., Sahoo, B. & Raghuwanshi, N. S. 2018 *Comparative Assessment of Model Uncertainties in Streamflow Estimation From A Paddy-Dominated Integrated Catchment-Reservoir Command*. AGU Fall Meeting, Washington, DC.

Dash, S. S., Sahoo, B. & Raghuwanshi, N. S. 2019 A SWAT-Copula based approach for monitoring and assessment of drought propagation in an irrigation command. *Ecological Engineering* **127C**, 417–430.

Efstratiadis, A., Tegos, A., Varveris, A. & Koutsoyiannis, D. 2014 Assessment of environmental flows under limited data availability: case study of the Acheloos River, Greece. *Hydrol. Sci. J* **59** (3–4), 731–750.

Graham, R. L., Turner, M. G. & Dale, V. H. 1990 How increasing CO_2 and climate change affect forests. *BioScience* **40** (8), 575–587.

Green, W. H. & Ampt, G. A. 1911 Studies on soil physics, 1. The flow of air and water through soils. *Journal of Agricultural Sciences* **4**, 11–24.

Guntner, A., Krol, M. S., De Araujo, J. C. & Bronstert, A. 2004 Simple water balance modelling of surface reservoir systems in a large data-scarce semiarid region. *Hydrological Sciences Journal* **49** (5), 901–918.

Hargreaves, G. H. & Samani, Z. A. 1985 Reference crop evapotranspiration from temperature. *Trans. ASAE* **1** (2), 96–99.

Hassan, W. H. 2019 Climate change impact on groundwater recharge of Umm ER Raduma Unconfined Aquifer Western Desert, Iraq. *International Journal of Hydrology Science and Technology* doi:10.1504/IJHST.2020.10021823.

Hassan, W. H., Nile, B. K. & Al-Masody, B. A. 2017 Climate change effect on storm drainage networks by storm water management model. *Environmental Engineering Research* **22** (4), 393–400.

IPCC 2001: Climate change 2001: impacts, adaptation and vulnerability, Contribution of Working Group II to the Third Assessment Report of the Intergovernmental Panel on Climate Change (J. J. McCarthy, O. F. Canziani, N. A. Leary, D. J. Dokken & K. S. White, eds). Cambridge University Press, Cambridge, UK, and New York, USA, pp 1032.

IPCC 2013 *Climate Change 2013: The Physical Science Basis. Contribution of Working Group I to the Fifth Assessment*

Report of the Intergovernmental Panel on Climate Change. Cambridge University Press, Cambridge.

Islam, A., Sikka, A., Saha, B. & Singh, A. 2012 Streamflow response to climate change in the Brahmani River Basin, India. *Water Resources Management* **26** (6), 1409–1424.

Jeong, D. L. & Kim, Y. O. 2005 Rainfall-runoff models using artificial neural networks for ensemble streamflow prediction. *Hydrological Sciences Journal* **19**, 3819–3853.

Jha, R., Sharma, K. D. & Singh, V. P. 2008 Critical appraisal of methods for the assessment of environmental flows and their application in two river systems of India. *KSCE Journal of Civil Engineering* **12** (3), 213–221.

Kumar, G., Kumar, A., Nath, V., Pandey, S. D., Kumar, V., Purvey, S. K. & Kumar, P. 2017 Impact of climate change on litchi systems and its adaptation strategies. *Proceedings of Challenges and Options in Litchi Production and Utilization, Gyan Manthan* **6**, 78–86.

Lenhart, T., Eckhardt, K., Fohrer, N. & Frede, H. G. 2002 Comparison of two different approaches of sensitivity analysis. *Physics and Chemistry of the Earth* **27**, 645–654.

Liang, X., Lettenmaier, D. P., Wood, E. F. & Burges, S. J. 1994 A simple hydrologically based model of land surface water and energy fluxes for general circulation models. *Journal of Geophysical Research: Atmospheres* **99**, 14415–14428.

Monteith, J. L. 1965 Evaporation and environment. In: *The State and Movement of Water in Living Organisms* (G. F. Fogg, ed.). Cambridge University Press Cambridge, UK, pp. 205–234.

Moriasi, D. N., Arnold, J. G., Van Liew, M. W., Bingner, R. L., Harmel, R. D. & Veith, T. L. 2007 Model evaluation guidelines for systematic quantification of accuracy in watershed simulation. *Trans ASABE* **50** (3), 885–900.

Nash, J. E. & Sutcliffe, J. V. 1970 River flow forecasting through conceptual models. Part I: a discussion of principles. *Journal of Hydrology* **10** (3), 282–290.

Neitsch, S., Arnold, J., Kiniry, J. & Williams, J. 2011 *Soil and Water Assessment Tool Theoretical Documentation Version 2009*. Texas Water Resources Institute, TR-406, pp. 1–647.

Padhiary, J., Patra, K. C., Dash, S. S. & Kumar, A. U. 2019 Climate change impact assessment on hydrological fluxes based on ensemble GCM outputs: a case study in eastern Indian River Basin. *Journal of Water and Climate Change*. https://doi.org/10.2166/wcc.2019.080.

Pandey, B. K., Gosain, A. K., Paul, G. & Khare, D. 2017 Climate change impact assessment on hydrology of a small watershed using semi-distributed model. *Applied Water Science* **19**, 2019–2041.

Perazzoli, M., Pinheiro, A. & Kaufmann, V. 2012 Assessing the impact of climate change scenarios on water resources in southern Brazil. *Hydrological Sciences Journal* **58** (1), 77–87.

Plangoen, P., Babel, M. S., Clemente, R. S., Shrestha, S. & Tripathi, N. K. 2013 Simulating the impact of future land use and climate change on soil erosion and deposition in the Mae Nam Nan sub-catchment, Thailand. *Sustainability* **5**, 3244–3274.

Priestley, C. H. B. & Taylor, R. J. 1972 On the assessment of surface heat flux and evaporation using large-scale parameters. *Monthly Weather Review* **100**, 81–92.

Sahoo, S., Khare, D., Mishra, P. K., Behera, S. & Krishan, R. 2016 A comparative study on environmental flows assessment methods in lower reach of Mahanadi river. *International Journal of Engineering Trends and Technology* **32** (2), 82–90.

Tripathi, M. P., Panda, R. K. & Raghuwanshi, N. S. 2003 Identification and prioritization of critical sub-watersheds for soil conservation management using the SWAT model. *Journal of Bio-Systems Engineering* **85** (3), 365–379.

USDA Soil Conservation Service 1972 *National Engineering Handbook*. U.S. Printing Office, Washington, D.C Section 4 Hydrology. Chapters 4–10.

van Griensven, A., Meixner, T., Grunwald, S., Bishop, T., Diluzio, A. & Srinivasan, R. 2006 A global sensitivity analysis tool for the parameters of multi-variable catchment models. *Journal of Hydrology* **324** (1–4), 10–23.

Van Vuuren, D. P., Edmonds, J., Kainuma, M., Riahi, K., Thomson, A., Hibbard, K., Hurtt, G. C., Kram, T., Krey, V., Lamarque, J. F., Masui, T., Meinshausen, M., Nakicenovic, N., Smith, S. J. & Rose, S. K. 2011 The representative concentration pathways. an overview. *Climatic Change* **109** (1–2), 5–31.

Whitehead, P. G., Wilby, R. L., Battarbee, R. W., Kernan, M. & Wade, A. J. 2009 A review of the potential impacts of climate change on surface water quality. *Hydrological Sciences–Journal–des Sciences Hydrologiques* **54** (1), 101–123.

Willmott, C. J., Robeson, S. M., Matsuura, K. & Ficklin, D. L. 2015 Assessment of three dimensionless measures of model performance. *Environmental Modelling and Software* **73**, 167–174.

Wischmeier, W. H. & Smith, D. D. 1978 *Predicting rainfall erosion losses: a guide to conservation planning*. Agriculture Handbook, US Department of Agriculture, Washington, DC, pp 58.

First received 24 September 2019; accepted in revised form 26 February 2020. Available online 21 April 2020